Study of mm-sized Coil to Coil Backscatter Based Communication Link

Xiao Sha
Department of Electrical and Computer Engineering
Stony Brook University
Stony Brook,USA
xiao.sha@stonybrook.edu

Yasha Karimi
Department of Electrical and Computer Engineering
Stony Brook University
Stony Brook,USA
yasha.karimi@stonybrook.edu

Samir R. Das
Department of Computer Science
Stony Brook University
Stony Brook,USA
samir@cs.stonybrook.edu

Petar Djurić
Department of Electrical and Computer Engineering
Stony Brook University
Stony Brook,USA
petar.djuric@stonybrook.edu

Milutin Stanaćević
Department of Electrical and Computer Engineering
Stony Brook University
Stony Brook,USA
milutin.stanacevic@stonybrook.edu

***Abstract*—Distribution of a large number of mm-sized sensing units in brain is a vision for the next generation of implantable devices for neural recording. Recorded data from the implants is conventionally transferred to a central external device and the bandwidth of the uplink channel is limited by the number of the implanted units. For the first time, we demonstrate the feasibility of local communication between mm-sized coils using backscattering technique which promises to reduce the requirement on the uplink bandwidth between the external device and the implants. To demonstrate the feasibility of the proposed link, two implanted coils located at 14 mm implantation depth are used with the distance between coils of 1.5 mm. The transmitting coil switches between two terminating impedance and the input voltage at the receiving coil is observed in the simulations with a triple-loop inductive link designed at 90 MHz. We show that the voltage difference in the received signal for two transmitting states can be resolved by demodulator of the receiving implant demonstrating the link feasibility. Several simulations show the functionality of the link under wide range of different angular and lateral misalignment.**

***Index Terms*—Wireless data communication, mm-sized coils, backscattered signal, implantable devices, inductive coupling.**

I. Introduction

A conventional approach for recording neural signals at high spatial ($\sim$ 100 μm) and temporal (fraction of ms) resolution employs wireless microelectrode arrays (MEAs) [1]–[4]. The number of channels in a MEA has grown to a few hundreds of electrodes [5]. However, due to scarring caused by penetration in the tissue over time, the effectiveness of MEAs for chronic implantation is limited [6]–[8]. To increase the overall area of the brain in which neural activity can be monitored and avoid tissue penetration, micro-electrocorticography has recently been adapted as less invasive alternative in form of flexible recording array [9] and as an array of single modular mm-sized implants [10], [11]. To cover a wide area of the brain, the number of these implants quickly grows. These implants, similarly to MEAs, cannot have any wired connections through the skin, and the power delivery and communication have to be transcutaneous. The wireless power delivery is based on either acoustics or electromagnetics principles [12], [13]. The power that can be delivered by an external device is greatly affected by the wireless channel, which is characterized by significant attenuation of acoustic and electromagnetic signals. Similarly, since recorded or summarized information has to be transmitted off the implants, the communication channel introduces its own impediments. When the power link is implemented as an electromagnetic link, either based on near-field or far-field, the uplink communication channel is commonly implemented by backscattering [14]–[16]. In the backscattering link, the implant modulates the terminating impedance of either the coil (near-field) or the antenna (far-field) and the modulated signal is sensed at the external devices. This modulation requires ultra-low power consumption at few picojoules per bit (pJ/b), but the data rate is limited to a few 100 kbps [17]. The rate limit is due to constraints in the quality factor of the channel, which is optimized for the power delivery. A higher data rate at the cost of few 10s pJ/b can be achieved through impulse radio ultrawideband (IR-UWB) radio [18]–[20], but with large peak transmission power, which limits the form-factor of the implantable device due to the need for some sort of storage mechanism.

A critical challenge in the design of the neural system composed of a large number of freely floating mm-sized implants is the bandwidth of the communication channel from the implants to an external device. Further, the increased functionality of the implants adds additional burden on the

This work was supported by the SUNY Center-Scale Proposal Planning and Development Grant Program.

978-1-7281-3885-5/19/$31.00 ©2019 IEEE

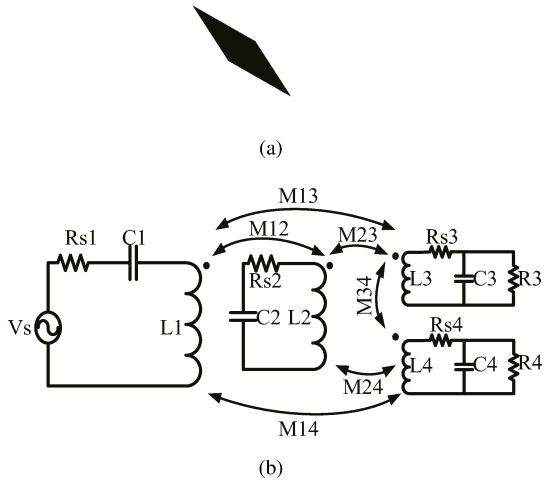

Fig. 1. (a)The triple-loop inductive link configuration for IMDs; (b)The circuit equivalent model of the inductive link

already limited power budget. With the small-form factor of the recording implants, the problem of packaging and biocompatibility is significantly alleviated.

An ambient backscattered system leverages the research for communication between several passive devices [21]. However, the power source is TV tower and their passive devices consumes large area, which are not suitable for implantable medical devices (IMDs). Here, we investigate the possibility for local communication between the mm-sized coils by backscattered signal, which can reduce the data exchange between external and internal coils. A triple-loop inductive link structure is implemented to increase the harvested power. Furthermore, the wide communication range shows the reliability of mm-sized coil to coil communication scenario. The rest of the paper is organized as follows: Section II describes the triple-loop inductive link design and discusses the optimum load chosen at coils. Section III presents the simulation result. Finally section V summarizes the novel contributions and proposes the future direction.

II. System Design

A. Optimal Coil Design

The implantable coil is modeled as 1 mm x 1 mm on chip coil implemented in 130 nm CMOS technology. The model consists of silicon substrate at the bottom, the copper spiral coil on the top of silicon substrate, and dielectric biocompatible coating materials(silicone). The coating material is used to decrease the parasitic resistance between coil and tissue, which can further increase the receiver coil quality factor [22]. The internal structures such as chip circuit and different layers in silicon substrate are neglected for the sake of simplicity.

A triple-loop inductive coupling structure [23] is utilized to improve transfer efficiency, the cover area and robustness against misalignment. Due to the small size of the implant chips, the optimization of the triple-loop inductive link can be divided into optimization of the two links each comprising 2-coils with a goal of maximizing the power transfer efficiency to the coil implanted at the specific implantation depth.

In the first step, the power transfer efficiency between mm-sized coil and resonator is increased by optimizing resonator and mm-sized coil through a 2-coil inductive link optimization procedure [24]. Starting with a set of realistic design constraints imposed by the strict size requirement of IMDs and printed circuit fabrication process, the optimal resonator and mm-sized coil geometries are determined by theoretical calculations [24]. In the next step, the geometry of the external coil is optimized to further increase coupling coefficient, and consequently maximize the power transfer efficiency between the external coil and the resonator without changing the geometry of the resonator. Further improvement can be achieved by iterating through the described procedure until the improvement for power transfer efficiency in an iteration becomes negligible. The geometrical parameters of the printed spiral coils on the FR4 and silicon substrate, such as track width, spacing, thickness and chip size are shown in Table I.

After obtaining the geometry of the coils through theoretical calculations, the coils with the dimensions shown in Table I are entered into 3D EM simulator ANSYS HFSS for further simulation. The external coil is excited following the limitation for safe tissue exposure to radio-frequency energy, which is 1.6 W/kg set by the Federal Communications Commission(FCC) in United States [25].

Figure 1(a) shows the cross-section of the EM simulation model of the two mm-sized coils, L_3 and L_4, along with a resonator coil, L_2 and a external coil, L_1, placed above six layers of the human tissue model [26]. The implanted transmitting coil, Imp(Tx), is aligned and kept at the center of the concentrating resonator and external coil. It is inserted into grey brain matter to mimic deep brain implantation scenario [27]. The distance and angle misalignment between Imp(Tx) and implanted receiving coil, Imp(Rx), is defined and shown in the Figure 1(b). The frequency-dependent dielectric properties of skin, fat, skull (bone), cerebrospinal fluid (CSF), dura, and brain are fed into this EM simulation model based on [28].

B. Backscattered Signal Calculation

The equivalent circuit model of the triple-loop inductive coupling link is shown in Figure 1(b). The highest power transfer efficiency(PTE) across inductive link can be achieved when all the LC tanks are tuned at the same resonance frequency, $f_0 = 1/2\pi\sqrt{L_1C_1} = 1/2\pi\sqrt{L_2C_2} = 1/2\pi\sqrt{L_3C_3} =$

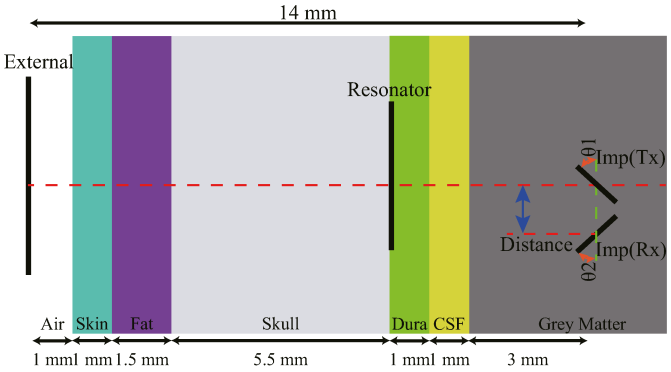

Fig. 2. Cross-section of the transcutaneous triple-loop inductive link including the six tissue layers.

TABLE I
CHARACTERIZATION OF EXTERNAL, $Imp(T_x)$, $Imp(R_x)$ COIL AND RESONATOR COIL

Parameter	External	Resonator	$Imp(T_x\&R_x)$
Diameter (mm)	12	9	1
Trace Width(μm)	1000	1000	200
Trace Thickness(μm)	34.7	34.7	4
Space between turns(μm)	200	NA	NA
Number of turns	2	1	1
Substrate Material	FR4	NA	sub130
Substrate Thickness(mm)	0.609	NA	0.5
SRF(GHz)	0.66	1.17	16.80
Operation Frequency(MHz)	90		

$1/2\pi\sqrt{L_4C_4}$. The effect of parasitic resistance in each coil circuit extracted from EM solver is denoted as R_{S1}, R_{S2}, R_{S3} and R_{S4}. C_1, C_2, C_3 and C_4 include the parasitic capacitance from tissue. R_3 and R_4 denote the terminating load in the implanted coils circuit.

The triple-loop inductive link with two mm-size coils can be model as the 4-ports Z-parameter network

$$\begin{bmatrix} V_1 \\ 0 \\ 0 \\ 0 \end{bmatrix} = \begin{bmatrix} Z_{11}^{'} & Z_{12} & Z_{13} & Z_{14} \\ Z_{21} & Z_{22}^{'} & Z_{23} & Z_{24} \\ Z_{31} & Z_{32} & Z_{33}^{'} + Z_{3L} & Z_{34} \\ Z_{41} & Z_{42} & Z_{43} & Z_{44}^{'} + Z_{4L} \end{bmatrix} \begin{bmatrix} I_1 \\ I_2 \\ I_3 \\ I_4 \end{bmatrix} \quad (1)$$

where $Z_{11}^{'}$, $Z_{22}^{'}$, $Z_{33}^{'}$ and $Z_{44}^{'}$ include the effect from the resonant capacitor in coil circuit. The optimum load further increases the PTE. It can be proved that

$$rZ_{3L}(opt) = rZ_{33} \quad (2)$$

if the Z_{11}, Z_{22}, Z_{33}, and Z_{44} are much larger than other components in the matrix and the imaginary part of the load impedance is resonant capacitor. The off-diagonal components indicate interaction between each coil. The received voltage and power at Imp(Rx) are given by $V_4 = Z_{4L}I_4$ and $P_4 = V_4^* I_4$. Although the highest PTE exists with an optimal load, the highest PTE and voltage at mm-sized coil are not achieved simultaneously. The increase of the load resistance leads to higher voltage at the output, and the sensitivity of the demodulator circuit also depends on the selection of the values of the load capacitance and load resistance [29]. A load resistance 1 kΩ is chosen.

To transmit data, Imp(Tx) coil switches between two load impedance. Two received signal levels are observed on the Imp(Rx) side corresponding to the "0" and "1" states on the Imp(Tx) side. As illustrated in the Figure 1(b), M_{34} represents the mutual inductance between Imp(Tx) and Imp(Rx) coils that can be estimated from the extracted Z parameter, Z_{34}. The reflected load theory(RLT) demonstrates the influence by an reflected impedance [30].

The maximal voltage change at the receiving side is achieved when the load in L_3 circuit switches from open to short. The voltage change across the load in L_4 circuit is defined as $\Delta V = V_{state1} \quad V_{state0}$. However, in order to allow the power transfer from the external coil to the Imp(Tx) coil in one state, in the loading state "1", instead of short circuit, the load is selected to be optimal for power transfer efficiency according to (2).

Our previous work demonstrated feasibility of a power efficient demodulator design that enables the receiver side of the RF tag-to-tag link to quantify the amplitude-shift keying(ASK) modulated signal with a modulation index as low as 0.6% with 1.5 mV voltage change. This sets the limit of the voltage difference that can be resolved at the receiving coil. The demodulator consists of a voltage doubler for envelope extraction and an amplifier with integrated filtering followed by comparator [26].

III. SIMULATION RESULTS

The mutual inductance between two loop coils depends on the proportion of flux generated by one loop that passes through the other loop. The mutual inductance of two square coils is:

$$\mathrm{M} = 1.1\times cos(\theta)\mu_0\pi\sqrt{R_1R_2}\int_0^\infty J_1(x\sqrt{\tfrac{R_1}{R_2}})J_1(x\sqrt{\tfrac{R_2}{R_1}})$$
$$\times J_0(x\tfrac{\rho}{\sqrt{R_1R_2}})exp(\quad x\tfrac{d}{\sqrt{R_1R_2}})dx$$

where R_1 and R_2 are coils radii, d is the center to center distance, ρ is lateral misalignment, θ is angle between two coils planes, J_0 and J_1 are the Bessel functions of the zeroth and first order [31]. The θ_1 and θ_2 in Figure 1(b) represent the angle between the external coil plane and internal coil planes, respectively. In the proposed scenario, the mutual inductance is maximum when $\theta_1 = \theta_2 = 90^o$ since in this case the aligned coils have the maximum overlap area.

The voltage difference observed at the receiving coil depends on both the mutual inductance between the implant coils and the received power at the transmitting coil, Imp(Tx). The receiving power at Imp(Tx) is minimum when $\theta_1 = 90^o$. We observe the trends in received voltage difference at Imp(Rx) with respect to different angles θ_1 and θ_2, as well as lateral misalignment, through simulations.

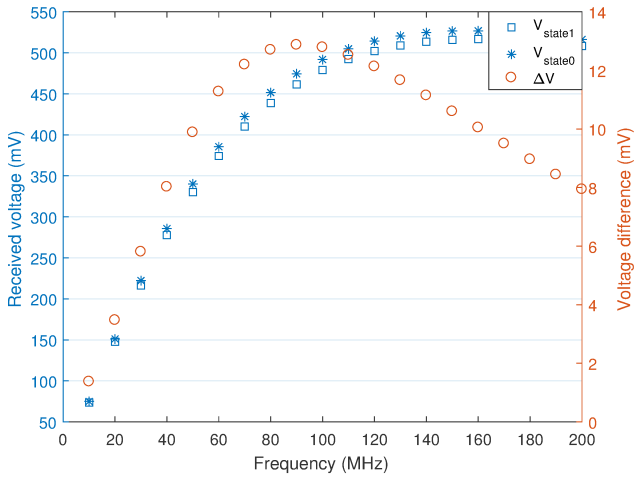

(a)

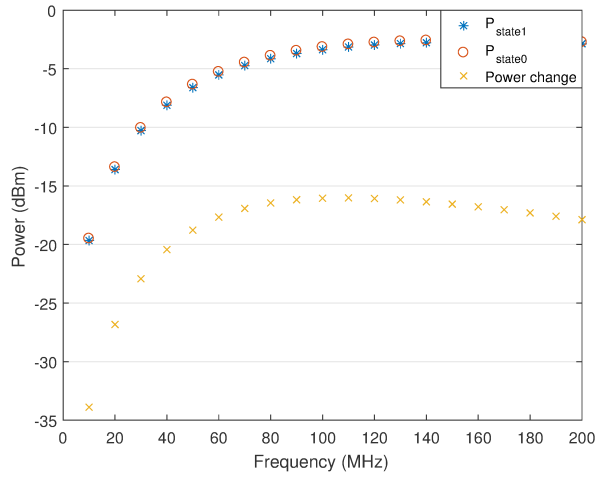

(b)

Fig. 3. Simulation result of the received power and voltage at Imp(Rx) in two state with $\theta_1 = 0°$, $\theta_2 = 45°$ and d = 1.5 mm as the function of operation frequency. (a) The received voltage and voltage difference at Imp(Rx) coil. (b) The received power and power difference at Imp(Rx) coil.

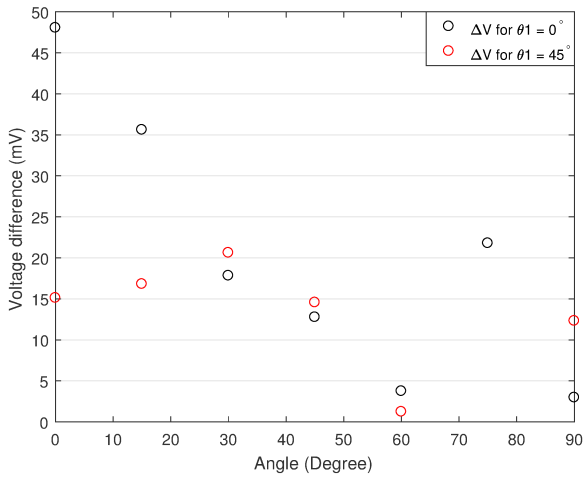

(a)

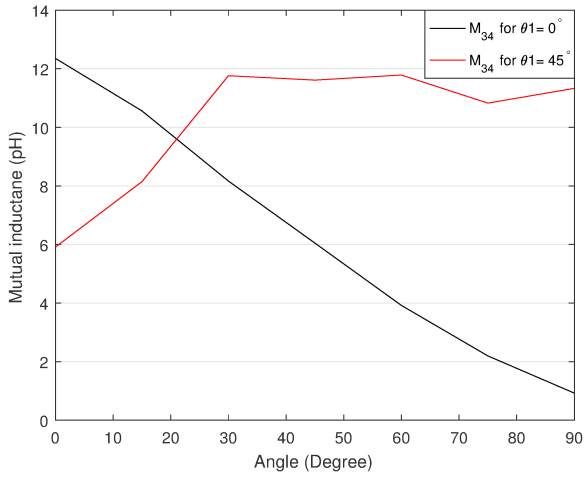

(b)

Fig. 4. (a)The voltage difference at Imp(Rx) and (b) mutual coupling coefficient M_{34} as the function of rotation angle θ_2 with d = 1.5mm at 90MHz.

A. *Frequency Analysis*

The reflected impedance from transmitting to receiving implant coil depends on the operational frequency due to the difference in the tissue absorption. In the first performed simulation, θ_1 is set to $0°$, θ_2 is set to $45°$ and the distance between the coils is set to 1.5 mm to mimic the curved brain surface. The input power to the external coil is 3.3 W, which is the maximum power that can be transmitted under the safety regulation. Figure 3(a) shows that the optimal point with the highest voltage difference at Imp(Rx), is reached at 90 MHz and that the voltage difference is 12.87 mV. As the frequency increases, the received power at Imp(Rx) coil starts saturating at 60 MHz and has maximum value of -2.56dBm at the 150 MHz, as shown in Figure 3(b). At the chosen operational frequency of 90 MHz, the received power is -3.46 dBm and -16.18 dB is the power difference. The SAR is 1.5 W/kg, which is slightly less than 1.6 W/kg and does not violate safe tissue exposure limitation.

B. *Angle Misalignment*

Two sets of angle misalignment simulation are performed. When Imp(Tx) is fixed with $\theta_1 = 0°$, Imp(Tx) coil has the largest mutual inductance with the external coil. When Imp(Tx) is rotated $45°$ with the respect to the external coil less magnetic flux pass through Imp(Tx), which reflects less power to Imp(Rx). On the other hand, the mutual inductance between implanted coils, M_{34}, depends on the angle difference between Imp(Tx) and Imp(Rx) $|\theta_2 \quad \theta_1|$ and on the overlapping area between coils as they are centered in the same plane, as illustrated in Figure 4(b). When $\theta_1 = 0°$, the voltage difference is larger than 1.5 mV at all the angles and ensures communication for different rotations of the receiving coil

as illustrated in Figure 4(a). Due to lower received power at Imp(Tx) for $\theta_1 = 45°$, the backscatter signal is weak and can not be resolved for $\theta_2 = 60^o$.

C. Lateral Misalignment

In order to find the maximum communication distance, we set θ_1 to $0°$ and $45°$ with $\theta_2 = 0°$ to mimic the sulci curvature of the brain. We assume that the distance between the coils is along the y-axis direction, as labeled in Figure 2, and the movement in the x-axis direction is defined as the lateral misalignment. In the Figure 5(a), the voltage difference at the receiving coil is shown as the function of distance with zero lateral misalignment for the two angles of Imp(Tx) coil. The voltage difference between two states is larger than 1.5 mV at all the points. When the lateral misalignment increases, the coil facing area is reduced. Figure 5(b) and Figure 5(c) show the relationship between voltage difference at the receiving coil and lateral misalignment of Imp(Rx) coil at three distance between coils for $\theta_1 = 0°$ and $\theta_1 = 45°$, respectively. In case when $\theta_1 = 0°$, voltage difference can still be demodulated up to 5.5 mm lateral misalignment with 4.5 mm distance. Even with the less magnetic flux from external coil, when $\theta_1 = 45°$, voltage change is larger than 1.5 mV when lateral misalignment is less than 4.5 mm at three distances, which ensure a 56.25% communication area coverage.

IV. Conclusion

We have proposed a mm-sized coil to coil communication link based on backscattering in order to enable local communication between implant coils. Investigation of the voltage change in the backscatter received signal has been performed in EM solver. This is the first demonstration of mm-sized coil to coil communication link. The demonstrated communication distance is 4.5 mm with 56.25% coverage area of the external coil. Clearly, a more careful inductive link design with uniform magnetic field distribution with external coil array [32] and current phase control circuit [26] could further improve the communication range. Next generation mm-sized coil to coil communication will incorporate multiple receiving coils in order to fulfill multi-channel mm-sized coil communication simultaneously.

References

[1] K. D. Wise, D. Anderson, J. Hetke, D. Kipke, and K. Najafi, "Wireless implantable microsystems: high-density electronic interfaces to the nervous system," *Proceedings of the IEEE*, vol. 92, no. 1, pp. 76–97, 2004.

[2] M. Yin, D. A. Borton, J. Aceros, W. R. Patterson, and A. V. Nurmikko, "A 100-channel hermetically sealed implantable device for chronic wireless neurosensing applications," *IEEE transactions on biomedical circuits and systems*, vol. 7, no. 2, pp. 115–128, 2013.

[3] X. Yun, D. Kim, M. Stanacevic, and Z. Mainen, "Low-power high-resolution 32-channel neural recording system," in *29th Annual International Conference of the IEEE Engineering in Medicine and Biology Society*, 2007, pp. 2373–2376.

[4] K. Murari, C. M. Sauer, M. Stanacevic, G. Cauwenberghs, and N. Thakor, "Wireless multichannel integrated potentiostat for distributed neurotransmitter sensing," in *27th Annual Conference of the IEEE Engineering in Medicine and Biology*, 2006, pp. 7329–7332.

[5] I. H. Stevenson and K. P. Kording, "How advances in neural recording affect data analysis," *Nature neuroscience*, vol. 14, no. 2, p. 139, 2011.

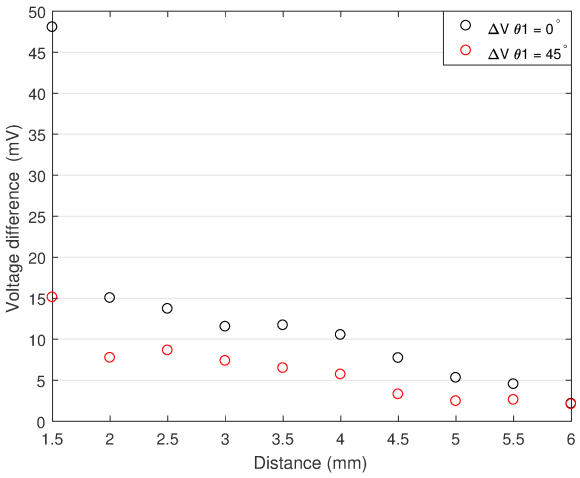

(a)

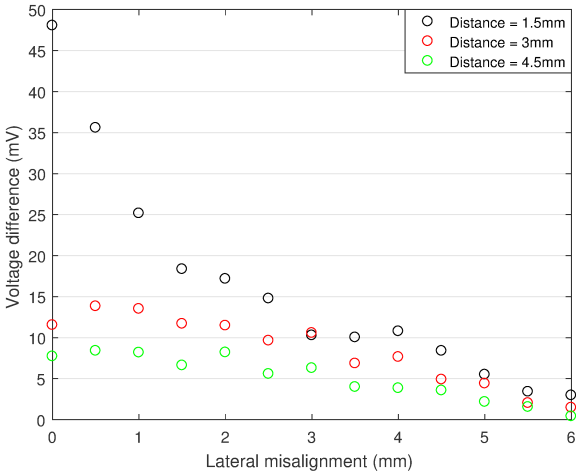

(b)

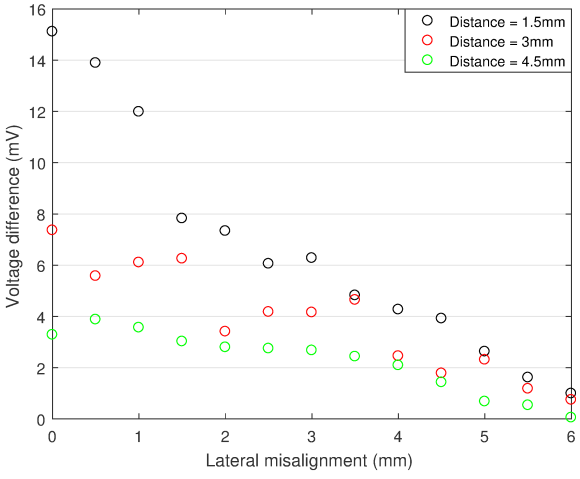

(c)

Fig. 5. The voltage difference at Imp(Rx) as (a)the function of distance with zero misalignment and the function of misalignment for (b) $\theta_1 = 0°$and (c) $\theta_1 = 45°$ with three distance at 90 MHz.

[6] G. C. McConnell, H. D. Rees, A. I. Levey, C.-A. Gutekunst, R. E. Gross, and R. V. Bellamkonda, "Implanted neural electrodes cause chronic, local inflammation that is correlated with local neurodegeneration," *Journal of neural engineering*, vol. 6, no. 5, p. 056003, 2009.

[7] A. Prasad, Q.-S. Xue, V. Sankar, T. Nishida, G. Shaw, W. J. Streit, and J. C. Sanchez, "Comprehensive characterization and failure modes of tungsten microwire arrays in chronic neural implants," *Journal of neural engineering*, vol. 9, no. 5, p. 056015, 2012.

[8] T. Saxena, L. Karumbaiah, E. A. Gaupp, R. Patkar, K. Patil, M. Betancur, G. B. Stanley, and R. V. Bellamkonda, "The impact of chronic blood–brain barrier breach on intracortical electrode function," *Biomaterials*, vol. 34, no. 20, pp. 4703–4713, 2013.

[9] B. Rubehn, C. Bosman, R. Oostenveld, P. Fries, and T. Stieglitz, "A mems-based flexible multichannel ecog-electrode array," *Journal of neural engineering*, vol. 6, no. 3, p. 036003, 2009.

[10] R. Muller, H.-P. Le, W. Li, P. Ledochowitsch, S. Gambini, T. Bjorninen, A. Koralek, J. M. Carmena, M. M. Maharbiz, E. Alon *et al.*, "A minimally invasive 64-channel wireless μecog implant," *IEEE Journal of Solid-State Circuits*, vol. 50, no. 1, pp. 344–359, 2015.

[11] S. Ha, A. Akinin, J. Park, C. Kim, H. Wang, C. Maier, P. P. Mercier, and G. Cauwenberghs, "Silicon-integrated high-density electrocortical interfaces," *Proceedings of the IEEE*, vol. 105, no. 1, pp. 11–33, 2017.

[12] J. S. Ho, S. Kim, and A. S. Poon, "Midfield wireless powering for implantable systems," *Proceedings of the IEEE*, vol. 101, no. 6, pp. 1369–1378, 2013.

[13] W. Biederman, D. J. Yeager, N. Narevsky, A. C. Koralek, J. M. Carmena, E. Alon, and J. M. Rabaey, "A fully-integrated, miniaturized (0.125 mm^2) 10.5 μw wireless neural sensor," *IEEE Journal of Solid-State Circuits*, vol. 48, no. 4, pp. 960–970, 2013.

[14] C. Sauer, M. Stanacevic, G. Cauwenberghs, and N. Thakor, "Power harvesting and telemetry in cmos for implanted devices," *IEEE Transactions on Circuits and Systems I: Regular Papers*, vol. 52, no. 12, pp. 2605–2613, 2005.

[15] S. Mandal and R. Sarpeshkar, "Power-efficient impedance-modulation wireless data links for biomedical implants," *IEEE Transactions on Biomedical Circuits and Systems*, vol. 2, no. 4, pp. 301–315, 2008.

[16] D. Jiang, D. Cirmirakis, M. Schormans, T. A. Perkins, N. Donaldson, and A. Demosthenous, "An integrated passive phase-shift keying modulator for biomedical implants with power telemetry over a single inductive link," *IEEE transactions on biomedical circuits and systems*, vol. 11, no. 1, pp. 64–77, 2017.

[17] S. Ha, C. Kim, J. Park, S. Joshi, and G. Cauwenberghs, "Energy-recycling integrated 6.78-mbps data 6.3-mw power telemetry over a single 13.56-mhz inductive link," in *VLSI Circuits Digest of Technical Papers, 2014 Symposium on*. IEEE, 2014, pp. 1–2.

[18] A. P. Chandrakasan, F. S. Lee, D. D. Wentzloff, V. Sze, B. P. Ginsburg, P. P. Mercier, D. C. Daly, and R. Blazquez, "Low-power impulse uwb architectures and circuits," *Proceedings of the IEEE*, vol. 97, no. 2, pp. 332–352, 2009.

[19] Y. Park and D. D. Wentzloff, "An all-digital 12 pj/pulse ir-uwb transmitter synthesized from a standard cell library," *IEEE Journal of Solid-State Circuits*, vol. 46, no. 5, pp. 1147–1157, 2011.

[20] P. P. Mercier, D. C. Daly, and A. P. Chandrakasan, "An energy-efficient all-digital uwb transmitter employing dual capacitively-coupled pulse-shaping drivers," *IEEE Journal of Solid-State Circuits*, vol. 44, no. 6, pp. 1679–1688, 2009.

[21] V. Liu, A. Parks, V. Talla, S. Gollakota, D. Wetherall, and J. R. Smith, "Ambient backscatter: Wireless communication out of thin air," *SIGCOMM Comput. Commun. Rev.*, vol. 43, no. 4, pp. 39–50, Aug. 2013. [Online]. Available: http://doi.acm.org/10.1145/2534169.2486015

[22] R. Erfani, F. Marefat, A. M. Sodagar, and P. Mohseni, "Modeling and characterization of capacitive elements with tissue as dielectric material for wireless powering of neural implants," *IEEE Transactions on Neural Systems and Rehabilitation Engineering*, vol. 26, no. 5, pp. 1093–1099, May 2018.

[23] M. Kiani, U. Jow, and M. Ghovanloo, "Design and optimization of a 3-coil inductive link for efficient wireless power transmission," *IEEE Transactions on Biomedical Circuits and Systems*, vol. 5, no. 6, pp. 579–591, Dec 2011.

[24] U. Jow and M. Ghovanloo, "Modeling and optimization of printed spiral coils in air, saline, and muscle tissue environments," *IEEE Transactions on Biomedical Circuits and Systems*, vol. 3, no. 5, pp. 339–347, Oct 2009.

[25] "Ieee standard for safety levels with respect to human exposure to radio frequency electromagnetic fields, 3 khz to 300 ghz," *IEEE Std C95.1, 1999 Edition*, pp. 1–83, April 1999.

[26] Y. Karimi, A. Khalifa, W. Montlouis, M. Stanaćević, and R. Etienne-Cummings, "Coil array design for maximizing wireless power transfer to sub-mm sized implantable devices," in *2017 IEEE Biomedical Circuits and Systems Conference (BioCAS)*, Oct 2017, pp. 1–4.

[27] A. Khalifa, Y. Karimi, Q. Wang, S. Garikapati, W. Montlouis, M. Stanaćević, N. Thakor, and R. Etienne-Cummings, "The microbead: A highly miniaturized wirelessly powered implantable neural stimulating system," *IEEE Transactions on Biomedical Circuits and Systems*, vol. 12, no. 3, pp. 521–531, June 2018.

[28] S. Gabriel, R. W. Lau, and C. Gabriel, "The dielectric properties of biological tissues: III. parametric models for the dielectric spectrum of tissues," *Physics in Medicine and Biology*, vol. 41, no. 11, pp. 2271–2293, nov 1996. [Online]. Available: https://doi.org/10.1088

[29] A. Athalye, J. Jian, Y. Karimi, S. R. Das, and P. M. Djurić, "Analog front end design for tags in backscatter-based tag-to-tag communication networks," pp. 2054–2057, May 2016.

[30] M. W. Baker and R. Sarpeshkar, "Feedback analysis and design of rf power links for low-power bionic systems," *IEEE Transactions on Biomedical Circuits and Systems*, vol. 1, no. 1, pp. 28–38, March 2007.

[31] C. M. Zierhofer and E. S. Hochmair, "Geometric approach for coupling enhancement of magnetically coupled coils," *IEEE Transactions on Biomedical Engineering*, vol. 43, no. 7, pp. 708–714, July 1996.

[32] J. Jian and M. Stanaćević, "Adaptive transmitting coil array for optimal power transfer in deeply implanted medical devices," in *2016 IEEE International Symposium on Circuits and Systems (ISCAS)*, May 2016, pp. 2030–2033.